ChemComm

RSC Publishing

COMMUNICATION

View Article Online
View Journal

# Preparation of a semiquinonate-bridged diiron(II) complex and elucidation of its geometric and electronic structures†

Cite this: DOI: 10.1039/c3cc42980f

Received 22nd April 2013,
Accepted 1st June 2013

DOI: 10.1039/c3cc42980f

www.rsc.org/chemcomm



Amanda E. Baum, Sergey V. Lindeman and Adam T. Fiedler*

**The synthesis and crystal structure of a diiron(II) complex containing a bridging semiquinonate radical are presented. The unique electronic structure of this $S$ = 7/2 complex is examined with spectroscopic (absorption, EPR, resonance Raman) and computational methods.**

*p*-Hydroquinone (1,4-dihydroxybenzene; HQ) and its substituted derivatives are important biological cofactors due to the ability to participate in multiple proton- and electron-transfers.[1] HQs undergo reversible one- and two-electron oxidations to yield semiquinone radicals (SQs) and quinones (Qs), respectively. These redox events typically involve loss of proton(s), such that the net reaction is H-atom transfer.[2] In biochemical processes, HQ cofactors are often associated with one or more redox-active metal ions. For instance, photosystem II incorporates two quinones ($Q_A$ and $Q_B$) that shuttle electrons away from the primary electron donor, $P_{680}$.[3] In close proximity to both quinones is a nonheme mononuclear Fe center, and recent spectroscopic studies have detected significant magnetic interactions between the high-spin Fe(II) center and semiquinone forms of $Q_A$ and $Q_B$.[4] In addition, substituted HQs are generated as part of the microbial breakdown of halogenated and nitro aromatic compounds. In these cases, the HQs are oxidatively degraded by ring-cleaving dioxygenases (HQ dioxygenases, HQDOs) with nonheme mono-iron active sites.[5] Even in these enzymes the electroactive nature of HQs is critical, since the key intermediate in the putative catalytic cycle is a superoxo–Fe(II)–semiquinonate complex.[6]

In the course of our efforts to develop synthetic models of HQDOs, we recently prepared the diiron(II) complex $[Fe_2(^{Ph2}Tp)_2(\mu\text{-DMHQ})]$ (**1**; Scheme 1), where DMHQ is the dianion of 2,5-dimethoxyhydroquinone and $^{Ph2}Tp$ is hydrotris(3,5-diphenylpyrazol-1-yl)borate(1−).[7] X-ray diffraction (XRD) analysis revealed that **1** is a centrosymmetric complex with two high-spin, five-coordinate Fe(II) centers linked by a closed-shell *p*-hydroquinonate ligand (the Fe···Fe separation is 8.15 Å). Here, the magnetic and electrochemical properties of **1** are examined in detail. We report that one-electron oxidation of **1** yields a unique diiron(II) complex, $[\mathbf{2}]^+$, containing a bridging *p*-semiquinonate ligand ($DMSQ^{\bullet-}$). The geometric and electronic structures of $[\mathbf{2}]^+$ are verified on the basis of crystallographic, spectroscopic, and computational methods. To the best of our knowledge, $[\mathbf{2}]^+$ is the first crystallographically-characterized complex to feature Fe(II) center(s) bound to a SQ radical.[8,9] The results therefore have the potential to advance our fundamental understanding of metal–SQ interactions in biological systems. Moreover, dinuclear complexes with "noninnocent" bridging ligands have attracted considerable attention lately due to their novel electronic and magnetic behavior;[10] this manuscript contributes a new member to this fascinating class of compounds.

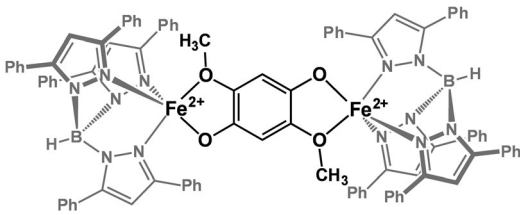


**Scheme 1** Structure of complex **1**.

Complex **1** is easily generated by mixing equimolar amounts of $FeCl_2$ and $K(^{Ph2}Tp)$ with 0.5 equiv. of $Na_2(DMHQ)$ in MeCN, followed by recrystallization from $CH_2Cl_2/Et_2O$.[7] The $^1H$ NMR spectrum of **1** in $CD_2Cl_2$, shown in Fig. S1 (see ESI†), reveals an abundance of paramagnetically-shifted peaks between $\delta$ = +60 and −20 ppm. Using the Evans method, an effective magnetic moment ($\mu_{eff}$) of 6.3 $\mu_B$ was measured at room temperature for **1**, which is reasonably close to the spin-only value of 6.93 $\mu_B$ expected for a molecule with two uncoupled high-spin ($S$ = 2) Fe(II) centers. Consistent with this result, broken symmetry (BS) calculations[11] using density functional theory (DFT) computed a $J$-value (exchange coupling parameter) of $-2$ cm$^{-1}$ for **1**, indicative of very weak antiferromagnetic interactions.[12]

The redox activity of **1** was examined in $CH_2Cl_2$ with 0.1 M $[NBu_4]PF_6$ as the supporting electrolyte. The cyclic voltammogram (CV) exhibits a reversible couple at $E_{1/2}$ = −570 mV *versus*

*Department of Chemistry, Marquette University, 535 N. 14th St., Milwaukee, WI 53233, USA. E-mail: adam.fiedler@marquette.edu; Fax: +1-414-288-7066*

† Electronic supplementary information (ESI) available: Experimental and computational details, and additional data. CCDC 934969 ([2]$PF_6$). For ESI and crystallographic data in CIF or other electronic format see DOI: 10.1039/c3cc42980f

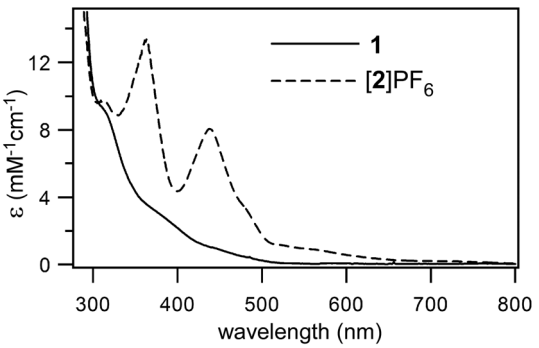


**Fig. 1** UV-visible spectra of **1** and $[\mathbf{2}]PF_6$ in $CH_2Cl_2$ at room temperature.

$Fc^{+/0}$ ($\Delta E$ = 130 mV), along with several irreversible events at more positive potentials (Fig. S2, ESI†). It is instructive to compare this CV to the one reported previously for [Fe($^{Ph2}$Tp)(2-MHQ)] (**3**; where 2-MHQ is the anion of 2-methoxyhydroquinone). Even though **1** and **3** feature nearly identical Fe coordination environments, the latter complex is oxidized at a much higher potential (−50 mV).[7] We therefore surmised that the −570 mV redox couple of **1** corresponds to a ligand-based event. To explore this possibility, complex **1** was treated with 1.0 equivalent of $AgPF_6$ in $CH_2Cl_2$. The resulting orange-brown species ($[\mathbf{2}]^+$) displays two intense absorption features with $\lambda_{max}$ = 365 and 440 nm ($\varepsilon$ = 13.2 and 8.0 $mM^{-1}$ $cm^{-1}$, respectively), along with shoulders at ∼480 and 540 nm (Fig. 1). Needle-like crystals of $[\mathbf{2}]PF_6$ were obtained by layering a concentrated $CH_2Cl_2$ solution with pentane.

The X-ray structure of $[\mathbf{2}]^+$ reveals a centrosymmetric diiron unit with the same atomic composition as **1** (Fig. S3, ESI†). Metric parameters for both complexes are provided in Table 1. The average Fe–$N_{Tp}$ bond length of $[\mathbf{2}]^+$ (2.094 Å) is only slightly shorter than the value observed for **1** (2.143 Å), suggesting that both Fe centers belong to the ferrous state. The Fe coordination environments are distorted between trigonal-bipyramidal and square pyramidal ($\tau$[13] = 0.34). The most dramatic structural changes upon conversion of **1** → $[\mathbf{2}]^+$ involve the bridging ligand. In the crystal structure of **1**, the C–C bond lengths of the $DMHQ^{2-}$ ligand are essentially identical (1.391 ± 0.004 Å) and the O1–C1 distance is 1.329(5) Å – typical values for *p*-hydroquinonate anions.[7] By contrast, the corresponding ring in $[\mathbf{2}]^+$ displays a pronounced quinoid distortion involving elongation of the C1–C2 and C1–C3 bonds and shortening of the C2–C3 bond. In addition, the O1–C1 distance of $[\mathbf{2}]^+$ contracts to 1.287(2) Å (Table 1). Such metric parameters require a semiquinone assignment for the bridging ligand in $[\mathbf{2}]^+$, based on well-established guidelines for the evaluation of dioxolene oxidation states.[14] Thus, the X-ray diffraction data support our hypothesis that oxidation of **1** is a ligand based process, such that $[\mathbf{2}]^+$ is best formulated as $[(Fe^{2+})_2(^{Ph2}Tp)_2(\mu\text{-DMSQ})]^+$.

**Table 1** Experimental and computed bond distances (Å) for **1** and $[\mathbf{2}]^{+a}$

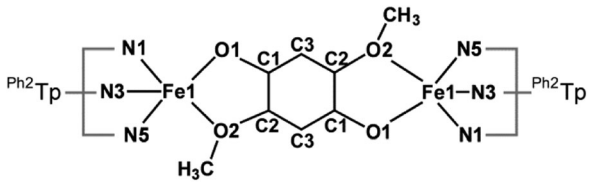


| | **1** (XRD) | $[\mathbf{2}]PF_6$ (XRD) | $[\mathbf{2}]PF_6$ (DFT) |
|---|---|---|---|
| Fe1–N1 | 2.107(4) | 2.125(2) | 2.072 |
| Fe1–N3 | 2.108(3) | 2.076(2) | 2.051 |
| Fe1–N5 | 2.213(4) | 2.082(2) | 2.067 |
| Fe1–O1 | 1.904(3) | 1.940(1) | 1.909 |
| Fe1–O2 | 2.328(3) | 2.403(1) | 2.682 |
| O1–C1 | 1.329(5) | 1.287(2) | 1.303 |
| O2–C2 | 1.388(6) | 1.358(2) | 1.360 |
| C1–C2 | 1.395(7) | 1.446(2) | 1.449 |
| C1–C3 | 1.388(6) | 1.415(2) | 1.419 |
| C2–C3 | 1.389(7) | 1.366(2) | 1.381 |
| $\tau$-Value[13] | 0.59 | 0.34 | 0.74 |

[a] Both **1** and $[\mathbf{2}]PF_6$ are centrosymmetric compounds.

The electronic structure of $[\mathbf{2}]PF_6$ was examined with spectroscopic and computational techniques. The X-band EPR spectrum exhibits a peak at $g_{eff}$ = 13.9 and a derivative-shaped feature at $g_{eff}$ = 5.4 (Fig. 2). Since half-integer spin systems cannot give rise to features with $g_{eff} > 4S$ (assuming real *g*-values near 2.0),[15] the EPR results suggest that $[\mathbf{2}]^+$ possesses a spin of 7/2. Indeed, as shown in Fig. 2, the data is nicely simulated assuming $S$ = 7/2 and the following spin-Hamiltonian parameters: $D$ = +7(2) $cm^{-1}$, $E/D$ = 0.11(2), and $g_{real}$ = 2.3, 2.2, 2.1.[16] These values were obtained by fitting EPR spectra measured at temperatures ranging from 5 to 20 K. The $g$ = 13.9 peaks therefore arises from the lowest-energy $M_S$ = ±1/2 doublet, while the derivative signal at 5.4 is due to the $M_S$ = ±3/2 doublet;[15] as expected, the former diminishes at higher temperatures while the latter gains in relative intensity (Fig. S4, ESI†).

The electronic origin of this unique EPR signal was elucidated with the aid of DFT. Using the crystallographic coordinates, a calculation with $S$ = 7/2 converged to a wavefunction consisting of two high-spin Fe(II) centers antiferromagnetically coupled to the bridging DMSQ radical (Fig. 3, left). Geometry optimizations indicate that this electronic configuration is the most stable one on the $S$ = 7/2 surface (bond distances for the optimized model are shown in Table 1). A *J*-value of −83 $cm^{-1}$ per Fe–DMSQ interaction was computed using the BS formalism.[17] Thus, unlike the closed-shell DMHQ ligand, the bridging radical in $[\mathbf{2}]^+$ is capable of mediating significant exchange interactions between the Fe-based spins, which are separated by 8.22 Å in the crystal structure. A similar spin topology was observed by Dei and Gatteschi for a *diferric* complex containing a bridging SQ ligand.[18] In this case, the overall spin is 9/2 and the *J*-value is considerably larger at −370 $cm^{-1}$.

The radical character of the $[\mathbf{2}]^+$ bridging ligand is illustrated by the singly-occupied molecular orbital (SOMO) shown in Fig. 3,

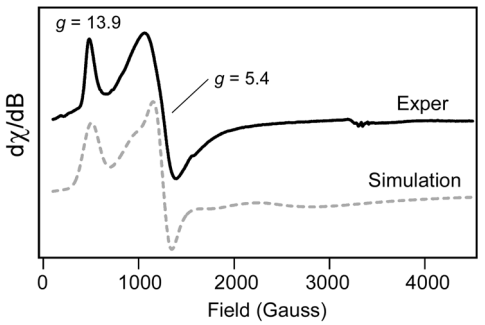


**Fig. 2** X-band EPR spectrum of $[\mathbf{2}]PF_6$ in a frozen $CH_2Cl_2$ solution (4 mM) collected at 10 K. Parameters used to generate the simulated spectrum are given in the text.

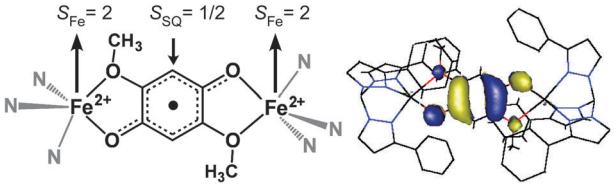


**Fig. 3** (Left) Spin coupling topology for $[2]^+$ that gives rise to overall spin of 7/2. (Right) DFT-generated isosurface plot of the $[2]^+$ SOMO.

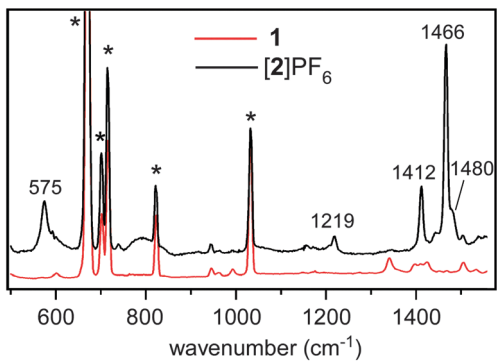


**Fig. 4** rR spectra of frozen $CD_2Cl_2$ solutions of **1** (red, bottom) and $[2]PF_6$ (black, top) obtained with 457.9 nm excitation. * = solvent peaks.

which is almost exclusively localized on DMSQ. This MO contributes to the intense electronic transitions that appear in the visible region, according to time-dependent DFT (TD-DFT) calculations that reproduce the experimental $[2]^+$ spectrum reasonably well (Fig. S5, ESI†). TD-DFT attributes the absorption manifold centered at 440 nm to multiple Fe(II) → DMSQ metal-to-ligand charge transfer (CT) transitions, while the higher-energy feature at 365 nm arises from a single DMSQ → Fe(II) ligand-to-metal CT transition. It appears that the existence of a ligand radical in $[2]^+$ is favored by the presence of low-symmetry, five-coordinate Fe(II) geometries, which stabilize the Fe 3d-orbitals and remove their degeneracy.[19]

The nature of the bridging ligand was further probed *via* resonance Raman (rR) spectroscopy. As shown in Fig. 4, the $[2]^+$ spectrum exhibits several intense peaks that are not evident in the precursor spectrum. The dominant feature at 1466 $cm^{-1}$ is strongly enhanced by excitation into 440 nm absorption feature (Fig. S6, ESI†), indicating that it corresponds to a DMSQ-based mode. The rR spectra of metal-bound *o*-dioxolenes typically display prominent peaks arising from C–O stretching modes. The frequencies of these modes are diagnostic of ligand oxidation state, appearing at 1250–1275 $cm^{-1}$ for catecholates, 1400–1500 $cm^{-1}$ for *o*-semiquinones, and 1620–1640 $cm^{-1}$ for *o*-benzoquinones.[14b] It is therefore reasonable to assign the dominant feature at 1466 $cm^{-1}$ to the symmetric $\nu$(O1–C1) mode of $[2]^+$. Literature precedents indicate that the 575 $cm^{-1}$ peak corresponds to the breathing mode of the five-membered chelates formed by each Fe center and the DMSQ ligand, while the resonance-enhanced peaks at 1412 and 1480 $cm^{-1}$ likely involve modes that strongly mix $\nu$(O1–C1) and intraligand C–C bond motions.[20] The rR data thus provides additional evidence for the presence of a DMSQ ligand in $[2]^+$.

The results presented here open up intriguing possibilities for future research. The fact that the ligand-to-metal and metal-to-ligand CT bands of $[2]^+$ appear in close proximity (*vide supra*) indicates that the Fe- and DMSQ-based orbitals are nearly isoenergetic, making it difficult to predict whether further oxidations would be ligand- or iron-centered. Studies are therefore underway to examine the electronic structure of the species generated *via* one-electron oxidation of $[2]^+$. In addition, we are developing mononuclear Fe(II)–semiquinonate complexes that mimic the putative catalytic intermediate of HQDOs.

The authors thank Dr Brian Bennett for allowing us to measure EPR data at the National Biomedical EPR Center (supported by NIH P41 Grant EB001980), and Thomas Brunold (Univ. Wisconsin) for access to his rR instrument. This research is supported by the National Science Foundation (CHE-1056845).

## Notes and references

1 (*a*) D. R. Weinberg, C. J. Gagliardi, J. F. Hull, C. F. Murphy, C. A. Kent, B. C. Westlake, A. Paul, D. H. Ess, D. G. McCafferty and T. J. Meyer, *Chem. Rev.*, 2012, **112**, 4016–4093; (*b*) R. G. Efremov and L. A. Sazanov, *Biochim. Biophys. Acta, Bioenerg.*, 2012, **1817**, 1785–1795.
2 (*a*) J. J. Warren, T. A. Tronic and J. M. Mayer, *Chem. Rev.*, 2010, **110**, 6961–7001; (*b*) M. H. V. Huynh and T. J. Meyer, *Chem. Rev.*, 2007, **107**, 5004–5064.
3 (*a*) F. Muh, C. Glockner, J. Hellmich and A. Zouni, *Biochim. Biophys. Acta, Bioenerg.*, 2012, **1817**, 44–65; (*b*) K. N. Ferreira, T. M. Iverson, K. Maghlaoui, J. Barber and S. Iwata, *Science*, 2004, **303**, 1831–1838.
4 (*a*) A. Sedoud, N. Cox, M. Sugiura, W. Lubitz, A. Boussac and A. W. Rutherford, *Biochemistry*, 2011, **50**, 6012–6021; (*b*) N. Cox, L. Jin, A. Jaszewski, P. J. Smith, E. Krausz, A. W. Rutherford and R. Pace, *Biophys. J.*, 2009, **97**, 2024–2033.
5 F. H. Vaillancourt, J. T. Bolin and L. D. Eltis, *Crit. Rev. Biochem. Mol. Biol.*, 2006, **41**, 241–267.
6 T. E. Machonkin and A. E. Doerner, *Biochemistry*, 2011, **50**, 8899–8913.
7 A. E. Baum, H. Park, D. N. Wang, S. V. Lindeman and A. T. Fiedler, *Dalton Trans.*, 2012, **41**, 12244–12253.
8 Min *et al.* reported a diiron(II) complex bridged by a chloranilate radical (ref. 9). However, this complex did not provide suitable crystals for X-ray crystallography.
9 K. S. Min, A. G. DiPasquale, J. A. Golen, A. L. Rheingold and J. S. Miller, *J. Am. Chem. Soc.*, 2007, **129**, 2360–2368.
10 (*a*) W. Kaim, *Inorg. Chem.*, 2011, **50**, 9752–9765; (*b*) J. S. Miller and K. S. Min, *Angew. Chem., Int. Ed.*, 2009, **48**, 262–272; (*c*) K. S. Min, A. G. DiPasquale, A. L. Rheingold, H. S. White and J. S. Miller, *J. Am. Chem. Soc.*, 2009, **131**, 6229–6236.
11 S. Sinnecker, F. Neese, L. Noodleman and W. Lubitz, *J. Am. Chem. Soc.*, 2004, **126**, 2613–2622.
12 K. Yamaguchi, Y. Takahara and T. Fueno, in *Applied Quantum Chemistry*, ed. V. H. Smith, Reidel, Dordrecht, 1986, p. 155.
13 A. W. Addison, T. N. Rao, J. Reedijk, J. Vanrijn and G. C. Verschoor, *J. Chem. Soc., Dalton Trans.*, 1984, 1349–1356.
14 (*a*) A. S. Attia, B. J. Conklin, C. W. Lange and C. G. Pierpont, *Inorg. Chem.*, 1996, **35**, 1033–1038; (*b*) A. Vlcek, *Comments Inorg. Chem.*, 1994, **16**, 207–228; (*c*) P. Chaudhuri, C. N. Verani, E. Bill, E. Bothe, T. Weyhermuller and K. Wieghardt, *J. Am. Chem. Soc.*, 2001, **123**, 2213–2223.
15 W. R. Hagen, in *Adv. Inorg. Chem.*, ed. R. Cammack, Academic Press, San Diego, CA, 1992, vol. 38, pp. 165–222.
16 Attempts to reproduce the data assuming a spin of 5/2 required unrealistically large $g_{real}$ values.
17 Experimentally, the variable-temperature EPR data (Fig. S4, ESI†) provides a lower-limit for the *J*-value. Since a signal from the $S = 5/2$ excited state is not observed in the 20 K spectrum, we can assume that its population is less than ~1% at this temperature. This requires a *J*-value greater than −40 $cm^{-1}$.
18 A. Dei, D. Gatteschi, L. Pardi and U. Russo, *Inorg. Chem.*, 1991, **30**, 2589–2594.
19 M. M. Allard, J. A. Sonk, M. J. Heeg, B. R. McGarvey, H. B. Schlegel and C. N. Verani, *Angew. Chem., Int. Ed.*, 2012, **51**, 3178–3182.
20 (*a*) B. T. O. Holt, M. A. Vance, L. M. Mirica, D. E. Heppner, T. D. P. Stack and E. I. Solomon, *J. Am. Chem. Soc.*, 2009, **131**, 6421–6438; (*b*) F. Hartl, D. J. Stufkens and A. Vlcek, *Inorg. Chem.*, 1992, **31**, 1687–1695.